Journal of Ceramic Processing Research. Vol. 12, No. 3, pp. 327~331 (2011)

J O U R N A L O F
Ceramic Processing Research

A comparison between hydrothermally prepared Co_3O_4 via H_2O_2 assisted and calcination methods

S. E. Hashemi Amiri, M. R. Vaezi* and A. Esmaielzadeh Kandjani
Division of Nanotechnology and Advanced Materials, Materials and Energy Research Center (MERC), Karaj, Iran.

In this paper Co_3O_4 nanoparticles were synthesized via two different synthesis procedures. In the first method, hydrothermally synthesized β-$Co(OH)_2$ particles were calcined at different temperatures. In the other method, H_2O_2 was used to eliminate the production of cobalt hydroxide. The amount of H_2O_2 was the main variable investigated in this study. All samples synthesized via these methods, were investigated for their structure, morphology, specific surface area and magnetization. The results showed that an increase in the temperature of the post heat treatment substantially increased particle sizes and consequently decreased the specific surface area of nanoparticles which influences magnetization. In the H_2O_2 assisted route, the minimum amount of the oxidant necessary for the complete elimination of the β-$Co(OH)_2$ phase and production of the pure Co_3O_4 phase was determined to be 0.25 volume fraction. In the H_2O_2 assisted method, due to elimination of the post heat treatment, the nanoparticles become smaller with a higher specific surface area in comparison with the calcination method. However, the magnetic properties of the nanoparticles in the H_2O_2 assisted method are influenced by changing the amount of H_2O_2.

Key words: Cobalt Oxide, Nanostructure, Hydrothermal Method, Magnetic Properties.

Introduction

Spinel structured nano- Co_3O_4 has attracted many researchers' attentions due to its significant properties. These properties make it as a promising candidate for different applications, such as: gas sensors [1], high-temperature solar selective absorbers [2], lithium batteries [3], catalysts [4] and magnets [5]. The performance of tricobalt tetraoxide particles in these applications strongly depends on the nanoparticles size and their specific surface areas [6, 7]. A high specific surface area with the smallest particle size become much more important where reaction kinetics is highly dependent on the active surface of the catalyst. Thus, many attempts have been made to synthesis a Co_3O_4 with a high specific surface area and low dimension, such as using sol-gel [8], chemical bath deposition (CBD) [9], chemical vapor deposition (CVD) [10] and hydrothermal methods [11]. Among these, the hydrothermal method has been used due to produce fine and uniform structures with high controllability in growth, and been used for the preparation of fine and uniform nano Co_3O_4 particles.

A simple hydrothermal synthesis at low temperature and low pressure, produces β-$Co(OH)_2$ instead of Co_3O_4. To produce cobalt oxide from the hydrothermal route, high pressures and temperatures should be provided [12]. Thus, when this simple synthesis method is used, always a post heat treatment should be performed to transform the β-$Co(OH)_2$ into Co_3O_4. Also the size of the nanoparticles is highly sensitive to temperature variations. In an alternative route for synthesizing Co_3O_4 via a hydrothermal method, appropriate amounts of oxidization agents such as H_2O_2 are added to produce Co_3O_4 at low temperatures and pressures so that no further calcinations are needed [13]. As discussed before, specific surface areas and the magnetic properties of the final product are highly dependant on the synthesis route; thus, an investigation of the properties of the nanoparticles obtained seems to be necessary.

In this paper, the influence of synthesis routes on the magnetic properties and surface area of Co_3O_4 nanoparticles has been studied. A simple hydrothermal method with post heat treatment and H_2O_2 assisted synthesis routes were investigated to obtain nano Co_3O_4 particles whose structure, morphology, specific surface area and magnetization were investigated using XRD, SEM, BET and VSM analysis, respectively.

Experimental

Materials

NH_4OH, H_2O_2 and $Co(Ac)_2$ (purchased from Merck) were used as the starting materials. They were of analytical grade and were used without further purification.

Synthesis route

Aqueous solutions of $Co(Ac)_2$ (0.1 M, 100 ml) and the desired amounts of H_2O_2 were added drop by drop to a NH_4OH aqueous solution for 30 minutes while the pH was adjusted to 10. The solution obtained was poured into 90 ml Teflon lined autoclaves and filled up to 80%

*Corresponding author:
Tel : +98-261-6210009
Fax: +98-261-6201888
E-mail: vaezi9016@yahoo.com

of their volume. Then the autoclaves were kept at 180 °C for 24 hours. After that, the autoclaves were cooled to room temperature naturally, and the precipitates were filtered and washed with distilled water and ethanol several times. Finally, the powders were dried at 50 °C for 24 hours. The samples which was synthesized in the absence of H_2O_2 was calcined at three different temperatures for 2 hours to obtain Co_3O_4. Table 1 lists process variables used in the current study.

Characterization

The structure of materials was studied using a Siemens D-5000 X-ray diffractometer (XRD) with Cu-Kα radiation (λ = 0.154178 nm). An scanning electron microscope (S360 Cambridge) was used to study the morphologies of the prepared samples. The specific surface area of the particles obtained were determined by Brunauer-Emmet-Teller method (BET-N_2 adsorption, Micromeritics Gemini 2375). The powder was degassed at 200 °C in a vacuum for 1.5 hours before the analysis. Simultaneous differential thermal analysis (DTA) was performed for samples synthesized in the absence of H_2O_2 with a thermal analyzer (STA 1640). The magnetic properties of the samples were characterized by vibrating sample magnetometer (VSM, AGSM).

Results and Discussion

The XRD patterns of the synthesized samples are shown in Fig. 1. The peaks are attributed to β-$Co(OH)_2$ (JCPDF 30-0443) and Co_3O_4 (JCPDF 42-1467) and no other peak was detected.

Mean crystallite sizes of the samples were estimated using Debye-Scherrer formula [14]:

$$D = \left(\frac{k\lambda}{\beta \cos\theta}\right) \quad (1)$$

where D is the mean crystallite size; k is a grain shape dependent constant (here assumed to be 0.89 for spherical particles); λ is the wavelength of the incident beam; θ is the Bragg angle; and β is the full width at half maximum (FWHM). For peaks related to $Co(OH)_2$, the (100) plane

Table 1. Synthesis variables used in this research

Sample	H_2O_2 (ml)	Calcination temperature (°C)
Co-0	-	-
Co-1	-	300
Co-2	-	600
Co-3	-	900
Co-4	5	-
Co-5	15	-
Co-6	25	-
Co-7	35	-
Co-8	45	-

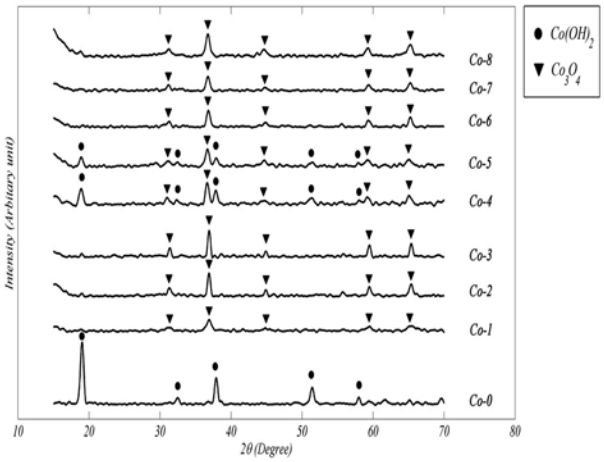

Fig. 1. XRD patterns of the synthesized samples.

was used for estimations; while for Co_3O_4, the (311) plane was used to determine the mean crystallite sizes.

Fig. 2 shows the differences between the final particle sizes for the two methods. As can be seen in this figure, an increase in calcination temperature increases the crystallite sizes drastically.

A calcination process is a common route for transforming a metal hydroxide into its metal oxide. This phenomenon can be explained via decomposition of hydroxide particles due to the heat imposed:

$$Co(Ac)_2 + 2(NK_4OH) \xrightarrow{Hydrothermal} Co(OH)_2\downarrow + dissolved\ remaining\ salt \quad (2)$$

$$3Co(OH)_2 + \frac{1}{2}O_2 \xrightarrow{\Delta} Co_3O_4 + 3H_2O\uparrow \quad (3)$$

The transformation was investigated using simultaneous thermal analysis. Fig. 3 illustrates the STA analysis of sample Co-0.

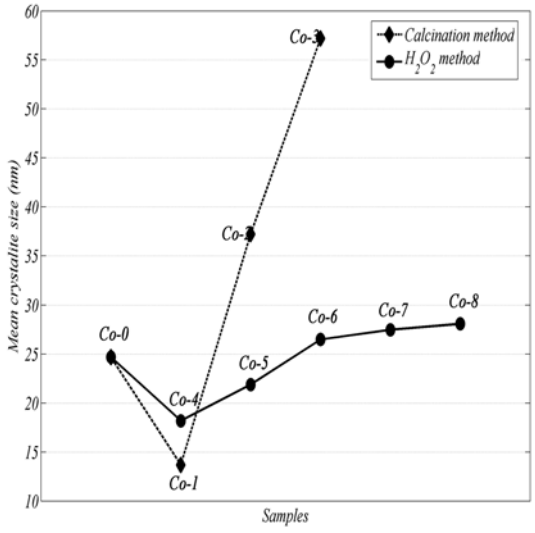

Fig. 2. Mean crystallite size of the Co_3O_4 samples. Co-0 ($Co(OH)_2$) is shown as a base to make the comparison more understandable.

Based on the DTA analysis, two distinct peaks can be observed for this sample. The first peak is endothermic (at 153 °C) and is related to the decomposition of $Co(OH)_2$ which results in the production of Co_3O_4. It is shown in the literature that the second peak (at 940 °C) is related to Co_3O_4 decomposition to CoO as follows [15]:

$$Co_3O_4 \xrightarrow{\Delta} CoO + \frac{1}{2}O_2 \quad (4)$$

In the current study, we focused on the production of Co_3O_4; therefore, the samples were not calcined above this temperature.

In the second procedure, an oxidizing agent was used in the hydrothermal process to change the degree of oxidation of cobalt in the reaction. In the absence of H_2O_2, considerable amounts of energy need to be provided to make the reaction change and the $Co(OH)_2$ transforms to Co_3O_4 or CoO from a thermodynamics point of view. In other words, by considering the unit cell theory in the hydrothermal synthesis process [16], there should be enough energy to make the $Co(OH)_2$ phase change into its complex form ($Co(OH)_4^{2-}$) and make a complex net of CoO or Co_3O_4.

When H_2O_2 was added to the reaction media, based on its concentration in the media, some Co^{2+} ions would change into Co^{3+} [17]. When Co^{3+} becomes available in the reaction media, the thermodynamic energetic barriers of ($Co(OH)_4^{2-}$) and subsequent complexes would be eliminated. But when the concentration of H_2O_2 is low, the oxidizing agent cannot fully change the degree of oxidation of all the available Co^{2+} and thus, just a portion of the starting material changes into Co_3O_4 and the remaining ions precipitate in the form of $Co(OH)_2$. This phenomenon can be seen in the XRD patterns (Fig. 1).

The SEM images for the calcination method are shown in Fig. 4. As may be seen in this figure, the morphologies of the particles and their agglomerated forms are different. When the $Co(OH)_2$ was calcined at 300 °C the particles tend to agglomerate in flakes, while the flakes seems to be faded by increasing the calcination temperature. at 850 °C, based on SEM images, further aggregation of the particles occurs by sintering the particles surfaces. By increasing the calcination temperature, the nanoparticles grow and thus bigger nanoparticles are produced.

In Fig. 5, SEM images of Co_3O_4 obtained via the H_2O_2

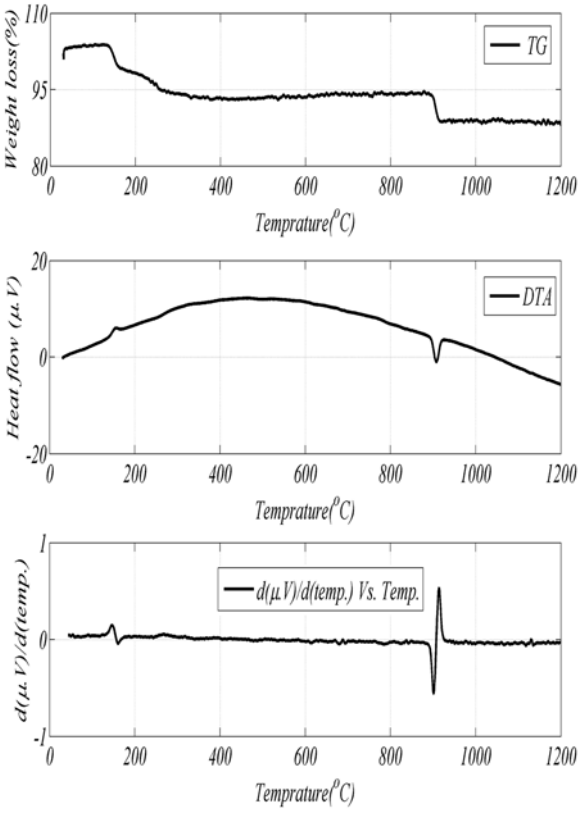

Fig. 3. STA analysis of sample Co-0.

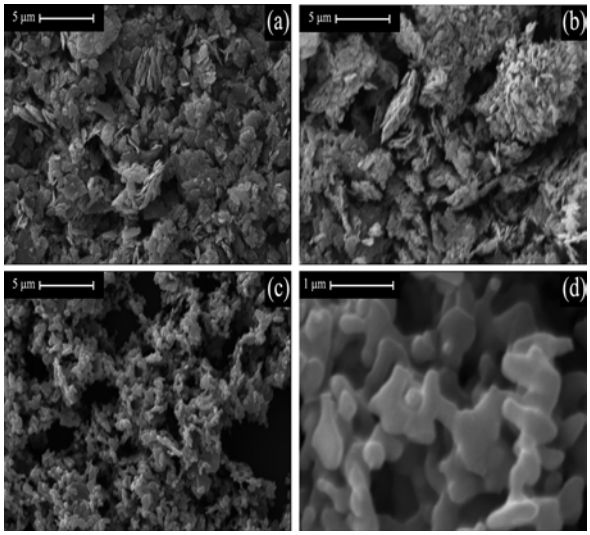

Fig. 4. SEM images of calcined samples at a) 300 °C (Co-1), b) 600 °C (Co-2) and c) 900 °C (Co-3); Image (d) shows the fractional surface sintered morphologies of Co_3O_4 nanoparticles.

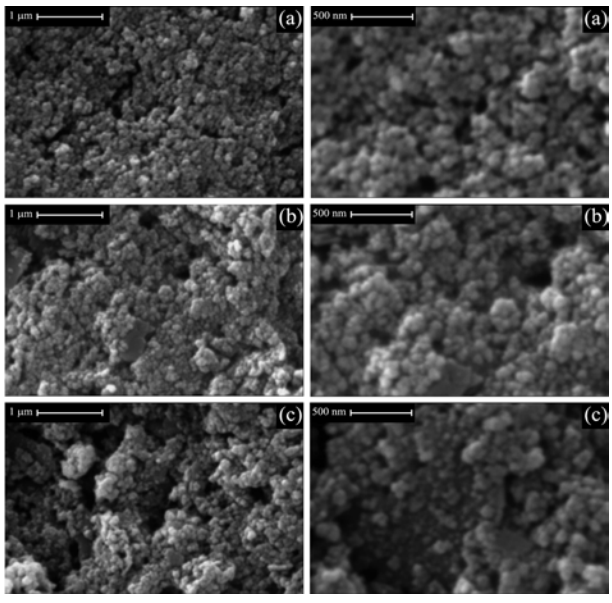

Fig. 5. SEM images of H_2O_2 assisted synthesized Co_3O_4 nanoparticles of samples a) Co-4, b) Co-6 and c) Co-8.

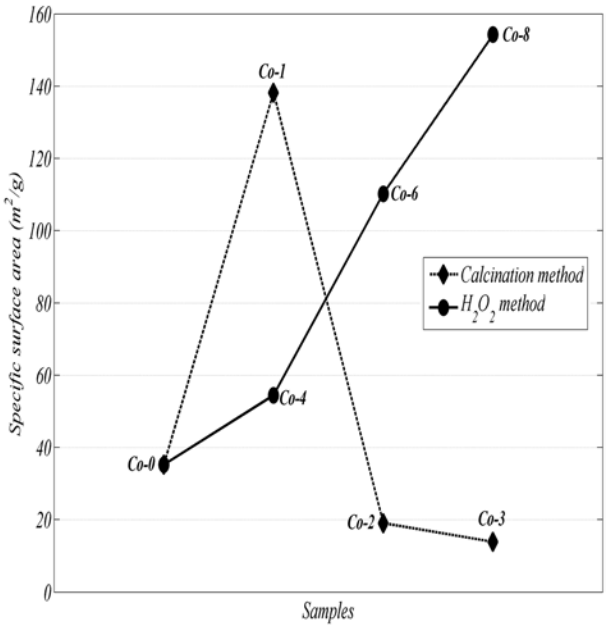

Fig. 6. Specific surface area of the samples.

method are shown. As can be seen in this figure, by increasing the amounts of H_2O_2, no considerable change can be detected in the morphologies of Co_3O_4 nanoparticles and their agglomerates.

By considering the morphologies, the specific surface areas of the particles should be different. The specific surface areas of the samples were calculated from the Brunauer-Emmett-Teller (BET) equation. The BET results for the samples are shown in Fig. 6.

As it can be seen in this figure, by decomposition of the $Co(OH)_2$ at 300 °C and its transformation to Co_3O_4, the surface area increases dramatically; but with a higher temperature heat treatment, due to the change in morphology from flake type to condensed aggregates the surface area decreases. By increasing the calcination temperature to 900 °C, due to an increase in crystallite and particle sizes and the fraction of sintering of the particles, the specific surface area shows a further decrease. When H_2O_2 is used for to synthesize Co_3O_4, the particles have the highest surface area. This could have arisen from the low temperature synthesis and also lower agglomeration of Co_3O_4 nanoparticles by this method.

The magnetic properties of nanoparticles are shown in Fig. 7. It demonstrates that all samples are antiferromagnetic and calcination did not change the magnetic behavior of the nanoparticles. The magnetization of cobalt hydroxide and samples Co-1, Co-2 and Co-3 is 0.10, 0.13 and 0.22 emu/g, respectively. Saturation did not occur and the coercivities of all the samples are about zero. It is seen that increasing the crystallite size causes an increase in magnetization.

The magnetic hysteresis loops of Co_3O_4 nanoparticles synthesized in the presence of H_2O_2 are illustrated in Fig. 7(b). The magnetization of samples Co-4, Co-6 and Co-8 were found to be 0.09, 0.18 and 0.34 emu/g, respectively. This shows that the behavior of the samples has changed gradually from Co-4 to Co-8 when more H_2O_2 is used in synthesizing the Co_3O_4 nanoparticles. With higher amounts of H_2O_2, a weak ferromagnetic behavior could be seen in the samples. This might be due to the existence of oxygen in the spinel structure of Co_3O_4 which avoids direct interaction of magnetic moments [18].

Conclusion

Using the different methods based on the hydrothermal synthesis of Co_3O_4, revealed the dependence of the

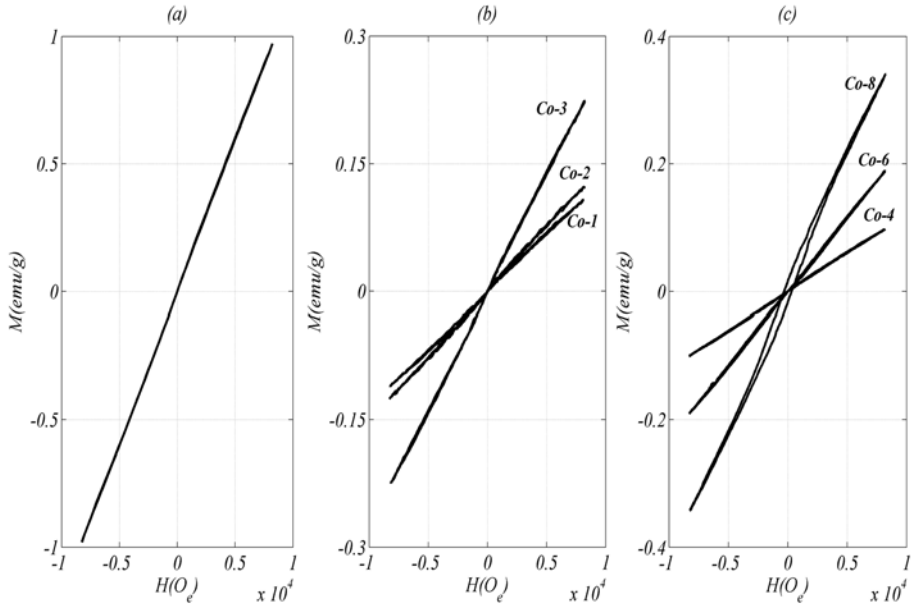

Fig. 7. Magnetic properties of the samples: a) Co-0, b) Calcination method and c) H_2O_2 assisted method.

nanoparticles to the synthesis route. The crystallite and particle sizes are increased with an increase in the heat treatment temperature. This phenomenon greatly decreases the specific surface area from 134 m^2/g to 13 m^2/g by changing the calcination temperature from 300 °C to 900 °C. Also, the magnetic properties of calcined nanoparticles depend on the post treatment temperature. In the H_2O_2 assisted method, the side effect of the post heat treatment of hydrothermally synthesized Co_3O_4 which decreases the specific surface area is eliminated. However, production of Co_3O_4 in the H_2O_2 assisted method is highly dependant on the amount of H_2O_2. If an inadequate amount of H_2O_2 is added to the synthesis media, the resulting structure would be a composite of β-$Co(OH)_2$ and Co_3O_4. With higher amounts of H_2O_2 the structure was pure Co_3O_4, however, the magnetic behavior of the particles becomes different due to the influence of oxygen on the spinel structure of the Co_3O_4.

References

1. S.D. Choi and B.K. Min, Sens. Actuat. B 77[1-2] (2001) 330-334.
2. K. Chidambaram, K.L. Malhotra and K.L. Chopra, Thin Solid Films 87[4] (1982) 365-371.
3. L.W. Yang, X.L. Na and Ch. Jun, J.Adv. Funct. Mater. 15[3] (2005) 851-856.
4. S. Fujita, K. Suzuki and T. Mori: Catal. Lett. 86[2] (2003) 139-144.
5. Y. Ichiyanagi, Y. Kimishima and S. Yamada, J. Magn. Mater. 272[2] (2004) 1245-1249.
6. C.B. Wanga, C.W. Tanga, S.J. Gaua and S.H. Chien, Catal. Lett. 101[3] (2005) 59-65.
7. R.V. Narayan, V. Kanniah and A. Dhathathreyan, J. Chem. Sci. 118[2] (2006) 179-184.
8. S. Thota, A. Kumar and J. Kumar, Mater. Sci. Eng. B 164[2] (2009) 30-35.
9. S.G. Kandalkar, J.L. Gunjakar, C.D. Lokhande and Oh-Shim Joo, J. Alloys Compd. 478[1-2] (2009) 594-598.
10. N. Bahlawane, E.F. Rivera, K. Kohse-Hoinghaus, A. Brechling and U. Kleineberg, Appl. Catal. B 53[3] (2004) 245-249.
11. P.E. Meskin, A.E. Baranchikov, V.K. Ivanov, E.V. Kisterev, A.A. Burukhin, B.R. Churagulov, N.N. Oleinikov, S. Komarneni and Yu.D. Tret'yakov, Dokl. Chem. 389[2] (2003) 62-67.
12. B. Basavalingu and J.A.K. Tareen, J. Mater. Sci. Lett. 5[1] (1986) 1227-1231.
13. Y.P. Yang, K.L. Huang, R.S. Liu, L.P. Wang, W.W. Zeng and P.M. Zhang, Trans. Nonferrous Met. Soc. China 17[1] (2007) 1082-1088.
14. B.D. Cullity, in "Elements of X-ray Diffraction" (Addison-Wesley, NewYork,1978) p. 158.
15. M. Chen, B. Hallstedt, L and J. Gauckler, J. Phase Equilib. 24[2] (2003) 212-217.
16. W.J. Li, E.W. Shi, W.Z. Zhong and Z.W. Yin, J. Crystal Growth 203[2] (1999) 186-191.
17. Y. You-ping, L. Ren-sheng, H. Ke-long, W. Li-ping, L. Su-qin and Z. Wen-wen, Trans. Nonferrous Met. Soc. China 17[1] (2007) 1334-1338.
18. D. Vollath, in "Nanomaterials" (Wiley-VCH, Germany, 2008) p. 45.